Journal of Applied Physics

Methodology and meaning of computing heat flux via atomic stress in systems with constraint dynamics

Cite as: J. Appl. Phys. **130**, 215104 (2021); https://doi.org/10.1063/5.0070930
Submitted: 10 September 2021 • Accepted: 15 November 2021 • Published Online: 03 December 2021

Donatas Surblys, Hiroki Matsubara, Gota Kikugawa, et al.

Journal of Applied Physics ARTICLE scitation.org/journal/jap

Methodology and meaning of computing heat flux via atomic stress in systems with constraint dynamics

Cite as: J. Appl. Phys. **130**, 215104 (2021); doi: 10.1063/5.0070930
Submitted: 10 September 2021 · Accepted: 15 November 2021 ·
Published Online: 3 December 2021

Donatas Surblys,[a] Hiroki Matsubara, Gota Kikugawa, and Taku Ohara

AFFILIATIONS

Institute of Fluid Science, Tohoku University, 2-1-1 Katahira, Aoba-ku, Sendai 980-8577, Japan

Note: This paper is part of the Special Topic on Engineering and Understanding of Thermal Conduction in Materials.
[a]**Author to whom correspondence should be addressed:** donatas@tohoku.ac.jp

ABSTRACT

Reliably obtaining thermal properties of complex systems, which often involves computing heat flux to obtain thermal conductivity via either Fourier's law or the Green–Kubo relation, is an important task in modern molecular dynamics simulations. In our previous work [Surblys *et al.*, Phys. Rev. E **99**, 051301(R) (2019)], we have demonstrated that atomic stress could be used to efficiently compute heat flux for molecules with angle, dihedral, or improper many-body interactions, provided a newly derived "centroid" form was used. This was later successfully implemented in the LAMMPS simulation package. On the other hand, small rigid molecules, like water and partial constraints in semi-flexible molecules, are often implemented via constraint force algorithms. There has been a lack of clarification if the constraint forces that maintain geometric constraints and can also be considered as many-body forces contribute to the overall heat flux and how to compute them correctly and efficiently. To address this, we investigate how to apply the centroid atomic stress form to reliably compute heat flux for systems with constraint or rigid body dynamics. We successfully apply the centroid atomic stress form to flexible, semi-flexible, and rigid water models; decompose the computed thermal conductivity into separate components; and demonstrate that the contribution from constraint forces to the overall heat flux and thermal conductivity is small but non-negligible. We also show that while the centroid formulation produces correct heat flux values, the original "group" formulation produces incorrect and sometimes unphysical results. Finally, we provide insight into the meaning of constraint force contribution.

I. INTRODUCTION

Molecular dynamics (MD) has been widely used as a numerical microscope, where the target systems are either too small or too ideal to be easily investigated via experimental approach. Mechanical and thermal properties can be computed relatively easily via statistical mechanics[1,2] but require correct computation of various thermodynamic quantities and their fluxes. Partly due to the rise of popularity of simulation packages such as the Large-scale Atomic/Molecular Massively Parallel Simulator (LAMMPS),[3] more complex systems are being widely targeted for investigation via MD. Unfortunately, while the dynamics of the systems are usually correct, the computation of thermal properties is not always correctly implemented. Specifically, it has been reported by our group, among others, that the "group" form atomic stress[4] used by LAMMPS is unfit to compute heat flux in systems with many-body interactions,[5–7] which originates from assumptions that only hold for pairwise interactions. As a solution, we proposed a new "centroid" form atomic stress that could be used to compute strictly correct system heat flux or give a good approximation of local heat flux.[6] The centroid atomic stress form has been successfully implemented in LAMMPS for angles, dihedrals, and impropers.

Small rigid molecules and partial constrains, such as fixed bond lengths, are often implemented via a family of constraint dynamics algorithms, of which SHAKE and RATTLE are most prominent.[8,9] The most notable example is water, which plays many important roles in both biological and industrial processes and is often implemented as a rigid body in MD.[10] At each

simulation step, constraint forces are computed and applied to each atom to fulfill given geometric constraints, which in case of water molecules are the OH bond lengths and the HOH angle. As the constraint forces on each atom can depend on several other atoms, they can be considered as many-body forces, therefore, the applicability of the group form atomic stress is questionable. Although the formulation for obtaining heat flux in rigid body dynamics has been long established,[11] not much attention has been given to constraint dynamics, where most researchers have opted to either obtain the mean heat flux indirectly form energy exchange with coupled thermostats or to impose specific heat flux directly on the system.[12,13] However, direct computation of instant heat flux might be necessary in some cases and is particularly important when one calculates thermal conductivity via the Green–Kubo relation, in which case the correct handling of constraint force contributions is crucial. In this work, we clarify if constraint forces contribute to the overall heat flux and demonstrate how to compute them reliably and efficiently. We do this by applying the centroid atomic stress formulation to these constraint forces and investigate if and how they contribute to the thermal properties, i.e., heat flux and thermal conductivity, of rigid and semi-flexible water molecules and compare them to a fully flexible water molecule. We also demonstrate how the original group atomic stress formulation is unfit for evaluating these constraint force contributions. In addition, to make the nature of the constraint force contribution clearer, we also consider rigid water molecules that are implemented via rigid body dynamics, i.e., by decoupling rigid body motion into translational and rotation components without directly using constraint forces.

II. SIMULATION AND ANALYSIS METHODS

The overall simulation conditions and analysis methods are similar to our previous work,[6] where we used square cuboid systems to determine thermal conductivity from both equilibrium molecular dynamics (EMD) and non-equilibrium molecular dynamics (NEMD) computations. All MD computations were made using the LAMMPS MD package,[3] with the velocity Verlet algorithm at a time step of 0.2 fs.

A. Potential models

Two water molecule potential models, one rigid and one flexible, were selected: the widely used is TIP3P,[14] and its flexible version that has harmonic bond and angle potentials, and is used in the multistate empirical valence bond model (MS-EVB),[15] which we denote as "TIP3P/Fs" for clarity and consistency as has also been done in other literature.[16] In case of the rigid TIP3P model, its equations of motion are usually solved via constraint dynamics by treating each atom as a point mass, in our case, via the RATTLE algorithm.[9] The equations of motion can also be solved by treating the TIP3P molecule as a rigid body and solving the rotational and translational motion separately. In such cases, we denote it as "TIP3P/rig," although strictly speaking both approaches produce rigid body motion and would result in identical trajectories, bar for numerical error. To also investigate semi-rigid molecules, we constructed a model where the bond lengths of TIP3P/Fs are constrained at their equilibrium lengths, while the angle is kept flexible and denote it as "TIP3P/Fs/cb."

The interaction between water molecules consists of van der Waals interactions, expressed by the Lennard-Jones (LJ) potential function with a simple cut-off distance, and electrostatic interactions due to partial charges on each atom. The sum of the LJ and Coulomb interactions will be referred to as "pair" interactions. The electrostatic interactions are expressed by a damped Coulomb potential developed by Fennell *et al.*,[17] which provides smooth decay of both energies and forces at a selected cut-off distance. Long-range electrostatic interactions were specifically avoided as they require different treatments[18,19] and would create extra ambiguity when computing local heat flux in control volumes, which is already an approximation as noted in our previous work.[6] The cut-off distance for both LJ and damped Coulomb potentials was set as 12 Å, while the damping coefficient for Coulomb potential was set to 0.2 $Å^{-1}$, which is a standard value.[17] Note that a rather technical and easily overlooked detail must be considered when comparing results obtained via constraint and rigid dynamics, such as TIP3P and TIP3P/rig. In many potential fields, including those used in this work, there are no LJ or Coulomb intra-molecular interactions, neither between neighboring atoms (1–2) nor between neighbors of neighbors (1–3). Simply excluding these interactions with damped or long-range Coulomb potentials would produce inconsistencies in energy computation and requires special treatment that is done automatically by LAMMPS if bond topology is present. Therefore, even for the TIP3P/rig model, bonds must be explicitly defined so that 1–2 and 1–3 interactions can be detected, even though it has no effect on the dynamics.

B. Simulation systems

For each of the four TIP3P, TIP3P/rig, TIP3P/Fs, and TIP3P/Fs/cb water models, an EMD and NEMD system was created, resulting in a total of eight simulation systems, each containing 6912 molecules. Simulation boxes were elongated in the z direction, and system dimensions were $5L \times 5L \times 20L$, with periodic boundary conditions set in all directions. The values of L that were used for production runs after equilibration are provided in Table I and correspond to systems at atmospheric pressure. The details of how system dimensions were obtained are given in Sec. II B 1.

TABLE I. Various simulation system properties. Brackets indicate standard error of mean, which was determined by dividing the data into 1 ns blocks to account for statistical inefficiency.[22]

Model	System	L (Å)	ρ(g/cm^3)	T(K)
TIP3P	NEMD	7.5128	0.975	300.12(2)
TIP3P	EMD	7.5122	0.975	299.16(1)
TIP3P/rig	NEMD	7.5128	0.975	300.14(5)
TIP3P/rig	EMD	7.5128	0.975	300.72(1)
TIP3P/Fs	NEMD	7.4046	1.019	300.22(3)
TIP3P/Fs	EMD	7.4042	1.019	297.64(2)
TIP3P/Fs/cb	NEMD	7.4482	1.001	300.12(3)
TIP3P/Fs/cb	EMD	7.4482	1.001	300.19(1)

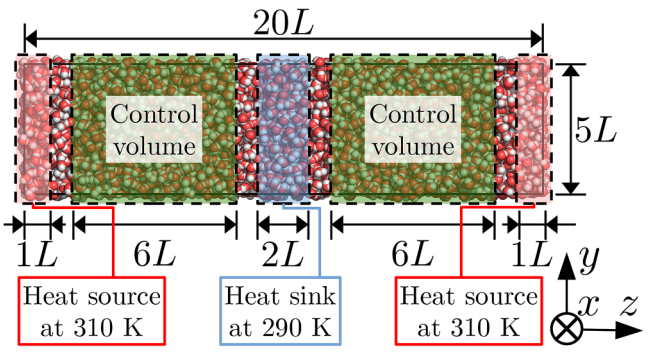

FIG. 1. Side view of the NEMD simulation system. The depth (x) dimension is the same as the height (y). The specific values of L are provided in Table I.

An overview of the NEMD system setup is shown in Fig. 1, where two Langevin thermostats[20] were used as heat source and heat sink at 310 and 290 K, respectively, with the damping coefficient set to 0.1 ps. To prevent random system drift, the gross random force of each thermostat was subtracted from the particles in the heat baths at each step. Two control volumes were set between the heat baths, where the heat flux is measured directly via atomic stress computation, as explained in Sec. II C. The EMD system setup is identical to that of NEMD, except there was no thermostating, i.e., NVE ensemble, and the whole system was used to measure the fluctuation of heat flux. The mean temperatures of all systems are provided in Table I.

Simulation systems used to determine system sizes, described in Sec. II B 1, were used as the initial condition after scaling them according to the L values in Table I, and they were equilibrated for 2 ns. The Nosé–Hoover style equations[21] were used to obtain NVT ensembles for EMD systems during equilibration, with otherwise identical settings to Sec. II B 1, while NEMD systems had identical settings to their production run. A following production run was conducted to sample heat flux values, which lasted at least 31 ns for NEMD systems and at least 13 ns for EMD systems.

1. Determining system sizes

To determine system dimensions, i.e., system density, under given temperature conditions at atmospheric pressure, TIP3P, TIP3P/Fs and TIP3P/Fs/cb were investigated under the Nosé–Hoover style equations[21] to produce either an NPT or NPH ensembles, corresponding to EMD and NEMD production systems, respectively, totaling in six different systems. The control temperature and pressure were set to 300 K and 1 atm, respectively, for NPT, while the control pressure was also set to 1 atm for NPH. The temperature and pressure damping coefficients were set to 0.1 and 1 ps, and the number of Nosé-Hoover chains for both thermostat and barostat were both 3. To maintain the desired temperature distribution for the NPH case, Langevin heat baths were coupled with the system as already described in Sec. II B and illustrated in Fig. 1. An equilibration of 0.2 ns was followed by sampling of 5 ns to determine the system density and dimensions. The standard error of mean of the density, determined from splitting the data into 1 ns blocks to account for statistical inefficiency,[22] was at most $0.0002\,\mathrm{g/cm^3}$.

As can be seen from the system dimensions and densities provided in Table I for TIP3P, TIP3P/Fs, and TIP3P/Fs/cb systems, there was very little to no difference between the NPT and NPH ensemble approaches, producing mostly identical densities. For the TIP3P/rig systems, same dimensions were adopted as TIP3P NEMD systems.

C. Computation of thermal conductivity

As described in our previous work,[6] a computationally efficient way to compute the precise global or an approximate local heat flux inside a control volume is via the atomic stress tensor

$$\vec{J}^{\Omega} \approx \frac{1}{\Omega}\left(\sum_{i\in\Omega}\vec{v}_i e_i - \sum_{i\in\Omega}\boldsymbol{\sigma}_i\cdot\vec{v}_i\right), \tag{1}$$

where e_i, $\vec{v}_i$, and $\boldsymbol{\sigma}_i$ are the energy, velocity vector, and atomic stress tensor of atom i and Ω denotes the control volume. The definition of $\boldsymbol{\sigma}_i$ is not unique, although often it is required that summing over all atoms is equivalent to system stress, which is uniquely defined via the virial theorem.[23] Another often desired property is the tensor being symmetric. In our previous work, we have demonstrated that the atomic stress tensor as originally implemented in LAMMPS, which we refer as the "group" atomic stress with details provided in Appendix C, produces unphysical results for many-body interactions, such as angle, bond, dihedral and improper potentials, when used to compute heat flux as in Eq. (1). We proposed an alternative "centroid" atomic stress formulation, which was free of such problems, although no longer symmetric. A brief description and derivation of centroid form atomic stress is provided in Appendix A.

Small rigid molecules, such as water, can be implemented either via constraint dynamics or rigid body dynamics, as described in Sec. II A. In each of these two approaches, the method for computing the contribution to atomic stress differs significantly. For constraint dynamics, LAMMPS designates a central atom to which up to other three atoms can connected via constrained bonds, where angle constraints are also converted to bond constraints. In such an atom cluster, the constraining forces contribute to atomic stress as

$$\boldsymbol{\sigma}_i^{\mathrm{group(cnstr.)}} = -\frac{1}{N_i}\sum_{\substack{j,l\in C_i\\ j<l}}\vec{r}_{jl}\otimes\vec{F}_{jl}^{\mathrm{cnstr.}}, \tag{2}$$

where C_i is the set of atoms that belong to the same cluster as atom i, $\vec{r}_{jl}$ is the displacement vector from atom l to atom j, $\vec{F}_{jl}^{\mathrm{cnstr.}}$ is the constraint force acting on j due to distance constraints with l, and N_i is the number of atoms in such cluster, specifically 2–4. From Eq. (2), we can see that the virial contribution from a constrained atom cluster is distributed equally to each participating atom, i.e., the constraints of the atom cluster are treated as a single many-body interaction. The expression for obtaining heat flux via the definition in Eq. (2) is provided in Appendix C, specifically Eqs. (C3)

and (C4). In case of rigid dynamics, the apparent constraint forces are computed for each atom that would be needed to satisfy the rigid body geometry, if the atoms were moving as independent mass points, and the contribution to atomic stress is as

$$\boldsymbol{\sigma}_i^{\text{group(cnstr./rig)}} = -\vec{r}_i \otimes \vec{F}_i^{\text{cnstr.}}, \tag{3}$$

where $\vec{r}_i$ and $\vec{F}_i^{\text{cnstr.}}$ are the position vector and apparent constraint forces of atom i. When comparing Eqs. (2) and (3), we can see that the approaches are quite different and participating atoms no longer get assigned identical virial contribution. Expression for obtaining heat flux via Eq. (3) definition can be found in Appendix C, Eq. (C5). In fact, strictly speaking, Eq. (3) does not follow the group formulation approach but will be referred as such for consistency. In addition, LAMMPS does not exactly follow Eq. (3), but stores only the upper triangular, and assumes a symmetric tensor. While this is true for the total system stress, it does not hold for per-atom virial stress. The implications of this will be discussed in Sec. III.

In accordance to our previous work, we define here the centroid atomic stress form for contributions to atomic stress from constraint and rigid dynamics. For constraint dynamics, we treat them the same as two-body potentials,

$$\boldsymbol{\sigma}_i^{\text{cntr(cnstr.)}} = -\frac{1}{2}\sum_{\substack{j\in C_i \\ j\neq i}} \vec{r}_{ij} \otimes \vec{F}_{ij}^{\text{cnstr.}}, \tag{4}$$

where the main difference with Eq. (2) is that contribution from constraint forces is considered only when atom i is directly involved. For example, in case of a water molecule, where i denotes the oxygen atom, Eq. (2) would also include the contribution due to constraint forces between hydrogen atoms, while Eq. (4) only includes constraint force contributions along the OH bonds. Expression for obtaining heat flux via Eq. (4) is in Appendix B, Eqs. (B5) and (B6). In case of rigid body dynamics, the contribution to centroid form atomic stress is defined as

$$\boldsymbol{\sigma}_i^{\text{cntr(cnstr./rig)}} = -\left(\vec{r}_i - \vec{r}_i^{\,0}\right) \otimes \vec{F}_i^{\text{cnstr.}}, \tag{5}$$

where $\vec{r}_i^{\,0}$ is the centroid position vector of the rigid body that contains atom i. Equations (3) and (5) are almost identical, except that the absolute positional vector is changed to a relative one. Equation (B7) in Appendix B provides the expression to obtain heat flux via Eq. (5). Strictly speaking, Eq. (4) is only easily applicable to constraint dynamics algorithms such as SHAKE and RATTLE,[8,9] where constraint forces along constrained bonds are readily available as part of the algorithm, and because angle constraints are converted into bond length constraints. For example, in case of water, OH bond length constraints and HOH angle constraints are actually implemented as two OH bond length constrains and one HH distance constraint. In this work, we assume that the kinetic energy exchange between two atoms due the constraint force occurring because of a length constraint between them is essentially the same as that of a pairwise interaction. This results in mostly identical treatment when computing heat flux, illustrated in Eqs. (B3) and (B5) in Appendix B. In other cases, such as the popular LINCS algorithm,[24] constraint forces along bonds are no longer part of the implementation and decomposing them into pairwise forces is not trivial. On the other hand, Eq. (5) is more generic and applicable to any constraint dynamics algorithm, including SHAKE, RATTLE, and LINCS, as computation of apparent constraint forces is trivial. While Eqs. (4) and (5) are not numerically identical, we will demonstrate that both approaches produce correct heat flux and thermal conductivity values.

In case of NEMD systems, mean system heat flux is also determined from the energy exchange with the Langevin thermostats and serves as a control value

$$\langle J_z \rangle = \frac{E^{\text{H}} - E^{\text{C}}}{2A_{xy}t}, \tag{6}$$

where E^{H} and E^{C} are the energy amounts that have increased and decreased in the system during t period due to the heat source and heat sink, respectively, while A_{xy} is the system cross-section area parallel to the xy plane, and $\langle\rangle$ brackets indicate time mean.

Either the group or centroid form of atomic stress is substituted into Eq. (1) to obtain the instant local or global heat flux values for NEMD and EMD systems, respectively, where the specific expressions for constraint force contributions are shown in Eqs. (2)–(5), while more detailed expressions are provided in Appendices A–C. For NEMD systems, Eq. (1) is summed over each of the two control volumes separately, indicated in Fig. 1, and the mean of z components is used, taking into account inverse heat flux signs. For EMD systems, Eq. (1) is summed over the whole system and all components are used, unless noted otherwise. In addition, Eq. (6) is also used for NEMD systems to act as a control value. From there either Fourier's law or the Green–Kubo relation is used to obtain thermal conductivity in NEMD and EMD systems, respectively,

$$\lambda = -\frac{\langle J_z \rangle}{\langle \nabla T_z \rangle}, \tag{7}$$

$$\lambda = \frac{1}{3VkT^2}\int_0^\infty \left\langle \vec{J}(t)\cdot\vec{J}(0)\right\rangle \mathrm{d}t, \tag{8}$$

where V, k, and T are system volume, Boltzmann's constant, and temperature, while $\langle \nabla T_z \rangle$ is the z component of the gradient of mean temperature distribution in NEMD systems. The mean temperature distribution is obtained via time mean, which is then linearly fitted in the control volume to obtain the temperature gradient. The first migrational term in Eq. (1) can be decomposed into kinetic and potential energy contribution, while the decomposition of the second virial term in Eq. (1) is described in Appendix B and C, and optionally consists of pair, bond, angle and constraint components. For NEMD systems, these components translate directly into contributions to thermal conductivity via Fourier's law in Eq. (7), while for the EMD systems, contributions to thermal conductivity are obtained via correlation between the

total heat flux and the specific component,[25]

$$\lambda^a = -\frac{\langle J_z^a \rangle}{\langle \nabla T_z \rangle}, \tag{9}$$

$$\lambda^a = \frac{1}{3VkT^2}\int_0^\infty \langle \vec{J}(t)\cdot\vec{J}^a(0)\rangle \, \mathrm{d}t, \tag{10}$$

where the "a" superscript indicates an arbitrary component.

III. RESULTS

The temperature distribution for the NEMD systems is shown in Fig. 2, where the lines are vertically shifted by multiples of 5 K for easier viewing. All of the models show similar temperature gradients due to identical thermostat settings and the temperature distribution is almost linear in the two control volumes. The heat flux values obtained from the Langevin thermostats, and the corresponding thermal conductivity values via Fourier's law in Eq. (7) are provided in Table II, which indicate that molecules with less constraints have higher thermal conductivity, which is reasonable considering the difference in degrees of freedom and has been reported in previous literature.[26] Our thermal conductivity values are higher than what has been reported experimentally at 300 K: 0.610(4) W/(m K).[27] On the other hand, thermal conductivity values for TIP3P and TIP3P/Fs water models at such temperature have been reported in literature as 0.88(2) and 1.063(1) W/(m K)[28,29] and are only slightly higher than the values in this work, which is most likely because we are using damped Coulomb interactions with a short cut-off of 12 Å as opposed to Ewald-based treatment of long-range electrostatics.[30,31]

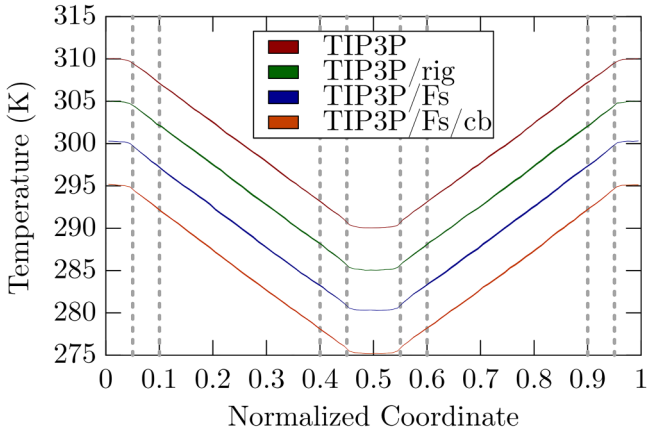

FIG. 2. Temperature distributions in NEMD simulation systems. Temperature values of TIP3P/rig, TIP3P/Fs, and TIP3P/Fs/cb are shifted by −5, −10, and −15 K for easier viewing. The thickness of each line varies along the *x* axis and is set to be twice the local standard error of mean, with the middle *y* value indicting the mean temperature. The standard error of mean was obtained by dividing data into 1 ns blocks to account for statistical inefficiency.[22] Vertical dashed lines indicate the heat source and sink regions, as well as control volumes, as illustrated in Fig. 1.

TABLE II. Heat flux values for NEMD systems and thermal conductivity values for all systems, where the "L," "g," and "c" superscripts indicate that heat flux was computed either via the Langevin thermostats or from group or centroid form of atomic stress, respectively. Brackets indicate standard error of mean, determined by dividing the data into 1 ns blocks to account for statistical inefficiency.[22]

Model	System	J^{L} (GW/m^2)	λ^{L} [W/(m K)]	λ^{g} [W/(m K)]	λ^{c} [W/(m K)]
TIP3P	NEMD	2.41	0.77(1)	0.68(2)	0.79(2)
TIP3P	EMD	N/A	N/A	0.86(1)	0.77(1)
TIP3P/rig	NEMD	2.41	0.78(1)	−143(2)	0.81(3)
TIP3P/rig	EMD	N/A	N/A	1.36(3)	0.80(1)
TIP3P/Fs	NEMD	2.83	0.89(1)	0.87(5)	0.94(5)
TIP3P/Fs	EMD	N/A	N/A	0.86(1)	0.91(1)
TIP3P/Fs/cb	NEMD	2.59	0.82(1)	0.75(3)	0.85(2)
TIP3P/Fs/cb	EMD	N/A	N/A	0.94(1)	0.84(1)

The decomposition of thermal conductivity obtained from all of the NEMD and EMD systems is shown in Fig. 3, where thermal conductivity obtained from temperature gradient and estimated heat flux from the heat baths in NEMD systems via Eq. (7) is shown as a gray dashed line to act as control, with width set to twice the size of standard error of mean. Dark horizontally shifted error bars indicate the error of mean of each component, while the horizontally centered red error bar at the top of each histogram bar indicates the overall error of mean, where they were evaluated by dividing data into blocks of 1 ns to account of statistical inefficiency.[22] The total and constraint error is not shown due to large magnitude, and only the *x* component data were used for group formulation of TIP3P/rig in NEMD (c) and EMD (d), respectively. The decomposition of thermal conductivity is done via Eqs. (9) and (10) for NEMD and EMD systems, respectively. From an overall view, only taking into account results that match the control values, we can conclude that most of heat is transferred via pairwise interactions, while migration terms (kinetic and potential energy) and angle or constraint force contributions are at the same level for flexible and rigid molecules.

First, we will describe results in detail concerning the rigid TIP3P and TIP3P/rig molecules. For TIP3P in Figs. 3(a) and 3(b), the group formulation underestimates the constraint contribution in both NEMD and EMD systems. The underestimation of constraint force contribution by the group formulation is similar to what has been shown for angle, dihedral, and improper potentials in our previous work.[6] In addition, the group form overestimates the overall thermal conductivity obtained via the Green–Kubo relation in the EMD system [Fig. 3(b)], where a similar trend for overestimation of overall thermal conductivity has also been previously observed in the EMD systems with angles, dihedrals, and impropers, although per-contribution tendencies are less consistent due to complicated relation in the correlation function. On the other hand, the centroid formulation provides a good match with the thermal conductivity obtained indirectly from the Langevin thermostat heat flux and indicates a non-negligible contribution from constraint forces. The NEMD underestimation and EMD overestimation by the group formulation are also present in TIP3P/rig, but

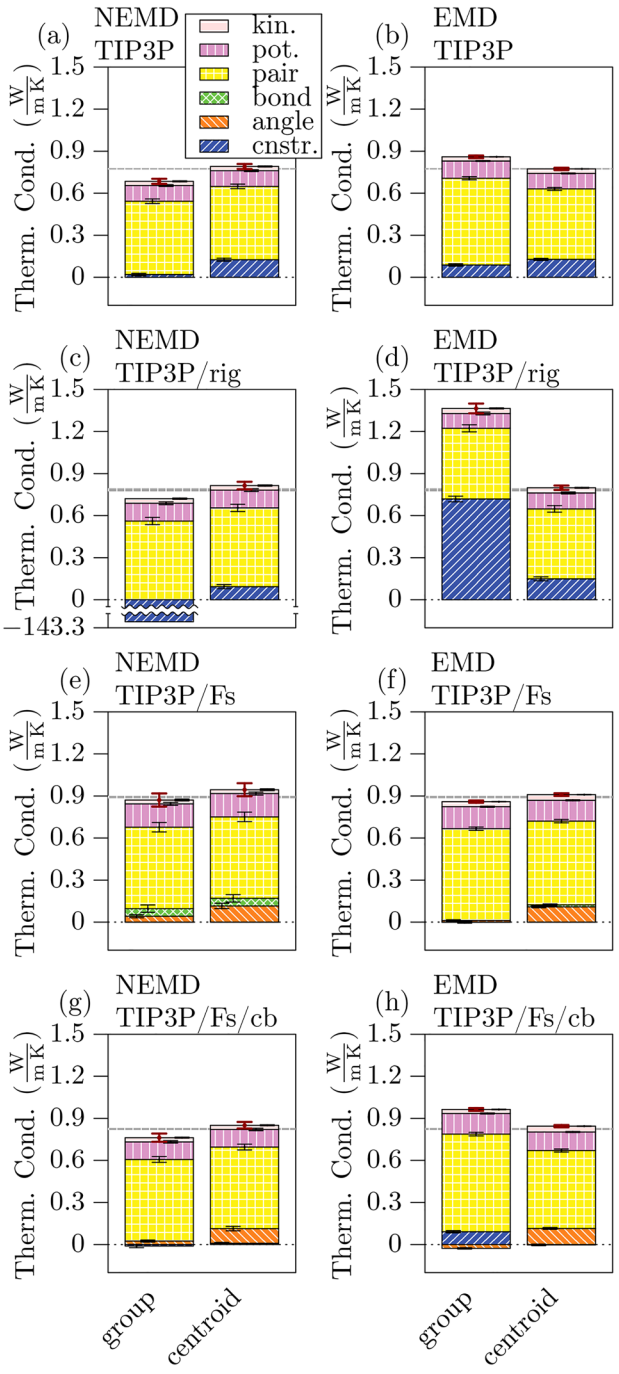

FIG. 3. Decomposition of thermal conductivity contributions under group and centroid atomic stress definitions for (a) TIP3P in NEMD, (b) TIP3P in EMD, (c) TIP3P/rig in NEMD, (d) TIP3P/rig in EMD, (e) TIP3P/Fs in NEMD, (f) TIP3P/Fs in EMD, (g) TIP3P/Fs/cb in NEMD, and (h) TIP3P/Fs/cb in EMD systems. The "kin." and "pot." notations indicate kinetic and potential contributions in the migration term, while "pair," "bond," "angle," and "cnstr." indicate inter-molecular pairwise, bond, angle, and constraint force contributions to the virial term.

to a much more extreme levels, especially for the NEMD system in Fig. 3(c), where the thermal conductivity is an unphysical negative value, as shown in Table II. The reason for this has been briefly touched when describing Eq. (3), but LAMMPS assumes a symmetric atoms stress tensor for rigid bodies and only stores the upper triangular. Due to this, only heat flux in the x direction is correctly computed via Eq. (3), while other components give unphysical results. This has been taken into account for EMD systems in Fig. 3(d), where only the x component was used, while the NEMD results are presented as is, as a complete reconstruction of the simulation system in the x direction would be required otherwise. Note that the unphysical results for the group formulation in Fig. 3(c) are due to LAMMPS implementation detail, and proper implementation of the group atomic stress as in Eq. (3) is expected to produce more physical, if not strictly correct, results. On the other hand, even when using only the x component for the TIP3P/rig system in Fig. 3(d), contributions from constraint forces are overestimated to an even bigger degree than they were for TIP3P. For further comparison, the time evolution of self-correlation integral of heat flux according to the Green–Kubo relation using only the x components is shown in Fig. 4, where the individual components are obtained via Eq. (10). We can clearly observe that the

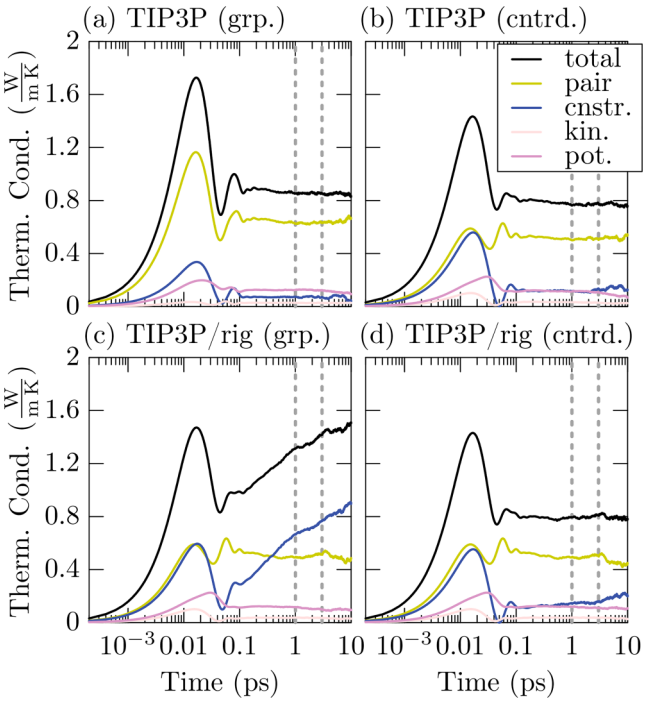

FIG. 4. Decomposed Green–Kubo integrals from EMD simulation systems for (a) TIP3P under group, (b) TIP3P under centroid, (c) TIP3P/rig under group, and (d) TIP3P/rig under centroid atomic stress formulation. Component notation is the same as in Fig. 3. Vertical dashed lines indicate regions from where the mean thermal conductivity values in Fig. 3 and Table II were obtained.

group formulation for TIP3P/rig does not converge, making it unfit for obtaining thermal conductivity from EMD systems.

To think about the nature of constraint force contributions, we first note an alternative formulation for the heat flux vector of rigid body molecules that can be divided into migrational, translational, and rotational terms,[11]

$$\vec{J} = \frac{1}{V}\left[\sum_i \vec{v}_i e_i + \frac{1}{2}\sum_{i\neq j}\vec{r}_{ij}\left(\vec{v}_i \cdot \vec{F}_{ij} + \vec{\omega}_i \cdot \vec{\tau}_{ij}\right)\right], \tag{11}$$

where $\vec{\omega}_i$ is principal angular velocity of molecule i and $\vec{F}_{ij}$ and $\vec{\tau}_{ij}$ are force and principal torque of molecule i due to interaction with molecule j. Also note that in Eq. (11), subscript i indicates the respective property of molecule i, while in other equations it refers to atom i. Specifically, $\vec{r}_{ij}$ in Eq. (11) is the displacement vector between molecule centers of mass, as opposed to that between atoms in previous equations. If we neglect the contribution of constraint forces and rewrite Eq. (1), due to only pairwise interactions remaining, the heat flux of rigid bodies such as TIP3P becomes

$$\vec{J}^{\text{w/o cnstr.}} = \frac{1}{V}\left[\sum_i \vec{v}_i e_i + \frac{1}{2}\sum_{i\neq j}\vec{r}_{ij}\left(\vec{v}_i \cdot \vec{F}_{ij}\right)\right], \tag{12}$$

where the i subscript refers to atom properties. In our earlier works, we have applied Eq. (11) to the SPC/E rigid water model[32] at 298 and 300 ;[33,34] therefore, we can conduct a qualitative comparison. We first compare the first term on the right-hand side, i.e., migration, in Eqs. (11) and (12) that is not dependent on the atomic stress definition. For both the rigid TIP3P and TIP3P/rig models in this work, and for the SPC/E model in the previous works, the migrational term via the atomic and molecular notation, respectively, composed a non-dominant part of the total heat flux. The specific numerical values somewhat differ, and while this could be due to difference in water models or handling of the Coulomb interactions, the inherent formulation is also different. The two expressions of the first term are not numerically identical: in Eq. (11), the total molecule energy is multiplied by the molecule velocity vector, while in Eq. (12), the energy of every atom is multiplied by its velocity vector. The second term provides an even starker difference. While the second term also looks similar, the summations are different. For example, in Eq. (11), $\vec{F}_{ij}$ is not necessarily parallel to $\vec{r}_{ij}$, while this is always true for Eq. (12). To illustrate this, consider a hypothetical water molecule model that is identical to TIP3P, except for partial charges, which are all 0. For two such molecules, there would only be LJ interaction between oxygen atoms with $\vec{F}_{ij}$ being parallel to the displacement vector between these two atoms, and almost never parallel to the displacement vector between the molecule centers of mass, resulting in different second term values in Eqs. (11) and (12). In our earlier work we have demonstrated that for the SPC/E water model, the third term on right-hand side of Eq. (11) is at least twice that of the second term at 300 K.[33] Therefore, the contributions from pair interactions, shown in Fig. 3 are substantially different when computed via the second term on the right-hand side of Eq. (11). Because both constraint and rigid body dynamics can produce identical systems, i.e., are simply different approaches to solving equations of motion, same heat flux values must be obtained regardless of formulation. As constraint forces are computed to fulfill geometric constraints that would break down when treating atoms as independent mass points, and because heat transfer inside rigid bodies is instantaneous, constraint force components of heat flux and thermal conductivity do not have a strong physical meaning. Indeed, the constraint force contribution can be seen as compensation for disregarding rigid constraints when computing pair contributions and possibly migration terms and neglecting the rigid rotation term in Eq. (11). It is not possible, however, to estimate the magnitude of the translational and rotational terms in Eq. (11) without computing them directly.

Finally, we take a look into a semi-flexible molecule TIP3P/Fs/cb, where only bond lengths are constrained and compare it with a fully flexible TIP3P/Fs in Figs. 3(e)–3(h). From the centroid formulation for NEMD systems in Figs. 3(e) and 3(g), we can observe that the constraint force contribution is almost negligible, while underestimation of angle contribution in the group formulation has been discussed in previous work.[6] Even in the flexible TIP3P/Fs model in Fig. 3(e), corresponding bond contributions are very small. An often used technique in MD simulation to only constrain bonds with hydrogen atoms.[35] Our results show that it might be acceptable to ignore constraint force contribution in such cases, although care should be taken when using the Green–Kubo relation in Eq. (8), as omitting even very small components could cause a breakdown in the relation. Regarding the EMD system of TIP3P/Fs/cb in Fig. 3(h), the group formulation overestimates the total thermal conductivity, as in previous systems. On the other hand, the group formulation for TIP3P/Fs in Fig. 3(f) underestimates thermal conductivity. While such underestimation has not been observed in this or previous work for other EMD systems, lack of consistency in either underestimating or overestimating individual contributions and large difference in degree of overall thermal conductivity overestimation when using group formulation indicates difficulty in determining general trends. On the other hand, the centroid formulation appears to produce consistent results within the margin of error for all cases.

IV. CONCLUSION

We showed that constraint forces in constraint dynamics must be considered when obtaining heat flux. We demonstrated that the centroid atomic stress formulation can be used to reliably obtain system and local heat flux in both equilibrium and non-equilibrium molecular dynamics for rigid and semi-flexible molecules and applied it to several different water molecule models. On the other hand, an earlier group atomic stress formulation that is implemented in LAMMPS produced erroneous and, in some cases, unphysical results. In rigid water molecules, the constraint forces had a non-negligible contribution to the overall heat flux and thermal conductivity, while in semi-flexible molecules where only bond lengths were fixed, the contributions were very small. This indicates that in systems where only bonds

containing hydrogen atoms are constrained, constraint force contribution might be discarded, provided special care is taken when applying the Green–Kubo relation.

These results are especially important when EMD systems are used to obtain thermal conductivity via the self-correlation of heat flux in the Green–Kubo relation, as improper evaluation of constraint force components, even when they are of small magnitude, causes incorrect estimation of the overall thermal conductivity values.

The authors plan to implement the centroid formulation in LAMMPS in the near future.

ACKNOWLEDGMENTS

This work was supported by JST CREST Grant No. JPMJCR17I2 and JSPS KAKENHI Grant No. 20K14659, Japan. Computational simulations were performed on the supercomputer system "AFI-NITY" at the Advanced Fluid Information Research Center, Institute of Fluid Science, Tohoku University.

AUTHOR DECLARATIONS

Conflict of Interest

The authors have no conflicts to disclose.

DATA AVAILABILITY

The data that support the findings of this study are available from the corresponding author upon reasonable request.

APPENDIX A: DERIVATION OF CENTROID FORMULATION

Here, we briefly give the general form and details on the derivation of the centroid atomic stress formulation. If interatomic forces only depend on atom positions and we assume equal potential energy distribution in many-body potentials, i.e., potential energy due to many-body interaction is distributed equally to each participating atom, the strictly correct system heat flux is[36]

$$\vec{J} = \frac{1}{V}\left[\sum_i \vec{v}_i e_i + \sum_{k=1}^{K} \frac{1}{N_k} \sum_{\substack{i,j\in k \\ j>i}} \vec{r}_{ij}\left(\vec{F}_i^k \cdot \vec{v}_j - \vec{F}_j^k \cdot \vec{v}_i\right)\right], \tag{A1}$$

where K is a set of many-body interactions, N_k is the number of atoms in the k-th many-body interaction, and $\vec{F}_i^k$ is the force on atom i due to that interaction. For convenience, we denote the second term inside the angle brackets on the right-hand side of Eq. (A1) as the virial component $\vec{Q}$ so that $\vec{J} = \frac{1}{V}\left(\sum_i \vec{v}_i e_i + \vec{Q}\right)$. As an example, we can expand the virial component of Eq. (A1) for only three-body interactions,

$$\begin{aligned}\vec{Q}^{3-\text{body}} &= \frac{1}{3}\sum_{\substack{k=1 \\ i,j,l\in k}}^{K(3-\text{body})} \vec{r}_{ij}\left(\vec{F}_i^k \cdot \vec{v}_i - \vec{F}_j^k \cdot \vec{v}_j\right) \\ &\quad + \vec{r}_{il}\left(\vec{F}_i^k \cdot \vec{v}_i - \vec{F}_l^k \cdot \vec{v}_l\right) \quad + \vec{r}_{jl}\left(\vec{F}_j^k \cdot \vec{v}_j - \vec{F}_l^k \cdot \vec{v}_l\right) \\ &= \frac{1}{3}\sum_{\substack{k=1 \\ i,j,l\in k}}^{K(3-\text{body})} \left(\vec{r}_{ij} + \vec{r}_{il}\right) \otimes \vec{F}_i^k \cdot \vec{v}_i \\ &\quad + \left(\vec{r}_{jl} - \vec{r}_{ij}\right) \otimes \vec{F}_j^k \cdot \vec{v}_j \quad + \left(-\vec{r}_{il} - \vec{r}_{jl}\right) \otimes \vec{F}_l^k \cdot \vec{v}_l. \end{aligned} \tag{A2}$$

As the centroid for the k-th three-body interaction in Eq. (A2) is $\vec{r}_0^k = (\vec{r}_i + \vec{r}_j + \vec{r}_l)/3$, we can show a simple relation for the sums of displacement vectors concerning the ith atom in Eq. (A2) by applying the $\vec{r}_j + \vec{r}_l = 3\vec{r}_0 - \vec{r}_i$ relation

$$\vec{r}_{ij} + \vec{r}_{il} = 3\vec{r}_{i0}^k, \tag{A3}$$

where $\vec{r}_{i0}^k$ indicates the displacement vector of i atom from the centroid position in the kth many-body interaction. Equivalent relation holds for other atoms, which lets us rewrite Eq. (A2) as

$$\begin{aligned}\vec{Q}^{3-\text{body}} = \sum_{\substack{k=1 \\ i,j,l\in k}}^{K(3-\text{body})} &\vec{r}_{i0} \otimes \vec{F}_i^k \cdot \vec{v}_i + \vec{r}_{j0} \otimes \vec{F}_j^k \cdot \vec{v}_j + \vec{r}_{l0} \otimes \vec{F}_l^k \\ &\cdot \vec{v}_l. \end{aligned} \tag{A4}$$

We want to express the virial component $\vec{Q}$ via atomic stress in the form of

$$\vec{Q} = -\sum_i \boldsymbol{\sigma}_i \cdot \vec{v}_i. \tag{A5}$$

By comparing Eqs. (A4) and (A5), we come to a natural definition of atomic stress tensor of each of the atoms in a single k-th three-body interaction as

$$\begin{aligned}\boldsymbol{\sigma}_i^{\text{cntr}(3-\text{body})} &= -\left(\vec{r}_i - \vec{r}_0^k\right) \otimes \vec{F}_i^k, \\ \boldsymbol{\sigma}_j^{\text{cntr}(3-\text{body})} &= -\left(\vec{r}_j - \vec{r}_0^k\right) \otimes \vec{F}_j^k, \\ \boldsymbol{\sigma}_l^{\text{cntr}(3-\text{body})} &= -\left(\vec{r}_l - \vec{r}_0^k\right) \otimes \vec{F}_l^k. \end{aligned} \tag{A6}$$

Equivalent derivation holds for many-body interactions of any size, resulting in the general formulation for centroid form of atomic virial stress tensor,

$$\boldsymbol{\sigma}_i^{\text{cntr}} = -\sum_{k\in K_i} \left(\vec{r}_i - \vec{r}_0^k\right) \otimes \vec{F}_i^k, \tag{A7}$$

where K_i is a set of many-body interactions that atom i participates in and the centroid vector is different for each many-body interaction k. As a special case, because $\vec{r}_{i0}^k = 0.5\vec{r}_{ij}$ and $F_i^k = F_{ij}^k$

for pairwise interactions, Eq. (A7) can be further simplified as

$$\boldsymbol{\sigma}_i^{\text{cntr(pair)}} = -\frac{1}{2}\sum_{\substack{k\in K_i \\ j\in k, i\neq j}} \vec{r}_{ij}\otimes\vec{F}_{ij}^{k}. \tag{A8}$$

In contrast to Eq. (A1), if we limit the summation of atomic stress in Eqs. (A7) and (A8) to a specific control volume, as in Eq. (1), the evaluated heat flux is no longer strictly correct, but still gives a good approximation as demonstrated in this and previous work.[6]

APPENDIX B: CENTROID VIRIAL HEAT FLUX COMPONENT DEFINITIONS

We provide specific definitions for virial components of heat flux $\vec{Q}$ when using centroid form atomic stress $\boldsymbol{\sigma}$. As a general expression, virial contribution to heat flux can be made up of the following components:

$$\vec{Q} = \vec{Q}^{\text{pair}} + \vec{Q}^{\text{bond}} + \vec{Q}^{\text{angle}} + \vec{Q}^{\text{cnstr.}}, \tag{B1}$$

where $\vec{Q}^{\text{pair}}$ is due to the pairwise LJ and Coulomb interactions, present for all water models; $\vec{Q}^{\text{bond}}$ is due to the harmonic bond potential only in TIP3P/Fs; $\vec{Q}^{\text{angle}}$ is due to the harmonic angle potential present in both TIP3P/Fs and TIP3P/Fs/cb, and $\vec{Q}^{\text{cnstr.}}$ is due to constraint forces in TIP3P, TIP3P/rig, or TIP3P/Fs/cb. The expression for pairwise potential contribution can be obtained by substituting Eq. (A8) into Eq. (A5),

$$\vec{Q}^{\text{pair}} = \frac{1}{2}\sum_{i<j}^{N}\vec{r}_{ij}\left[\left(\vec{F}_{ij}^{\text{LJ}} + \vec{F}_{ij}^{\text{Coul.}}\right)\cdot\left(\vec{v}_i + \vec{v}_j\right)\right], \tag{B2}$$

where we go over all atom pair combinations disregarding cut-off for brevity. Because the bond contribution is also a pairwise interactions, the expression is almost identical to Eq. (B2),

$$\begin{aligned}\vec{Q}^{\text{bond}} &= \frac{1}{2}\sum_{\substack{ij\in k \\ i<j}}^{K(\text{bond})}\vec{r}_{ij}\left[\left(\vec{F}_{ij}^{k(\text{bond})}\cdot\left(\vec{v}_i + \vec{v}_j\right)\right)\right] \\ &= \frac{1}{2}\sum_{\substack{m=1 \\ \text{O},\text{H}_1,\text{H}_2\in m}}^{M}\vec{r}_{\text{OH}_1}\left[\vec{F}_{\text{OH}_1}^{m(\text{bond})}\cdot\left(\vec{v}_{\text{O}} + \vec{v}_{\text{H}_1}\right)\right] \\ &\quad + \vec{r}_{\text{OH}_2}\left[\vec{F}_{\text{OH}_2}^{m(\text{bond})}\cdot\left(\vec{v}_{\text{O}} + \vec{v}_{\text{H}_2}\right)\right],\end{aligned} \tag{B3}$$

where the summation goes over all OH bonds in the first expression, and goes over every molecule m in the set of all water molecules M in the second expression. Angle contribution is identical to Eq. (A4) as

$$\begin{aligned}\vec{Q}^{\text{angle}} = &\sum_{\substack{k=1 \\ \text{O},\text{H}_1,\text{H}_2\in k}}^{K(\text{angle})}\vec{r}_{\text{O}0}\otimes\vec{F}_{\text{O}}^{k(\text{angle})}\cdot\vec{v}_{\text{O}} + \vec{r}_{\text{H}_1 0}\otimes\vec{F}_{\text{H}_1}^{k(\text{angle})}\cdot\vec{v}_{\text{H}_1} \\ &+ \vec{r}_{\text{H}_2 0}\otimes\vec{F}_{\text{H}_2}^{k(\text{angle})}\cdot\vec{v}_{\text{H}_2},\end{aligned} \tag{B4}$$

where the summation goes over all HOH angles and summation over water molecules would be identical, as each water molecule has at most one 3-body angle interaction. The constraint contribution is different depending on the water model. For TIP3P/Fs/cb, the expression is obtainable by substituting Eq. (4) into Eq. (A5), which results in simply replacing bond potentials with constraint forces, producing a similar expression to Eq. (B3),

$$\begin{aligned}\vec{Q}^{\text{cnstr.(TIP3P/Fs/cb)}} = &\frac{1}{2}\sum_{\substack{m=1 \\ \text{O},\text{H}_1,\text{H}_2\in m}}^{M}\vec{r}_{\text{OH}_1}\left[\vec{F}_{\text{OH}_1}^{m(\text{cnstr.})}\cdot\left(\vec{v}_{\text{O}} + \vec{v}_{\text{H}_1}\right)\right] \\ &+ \vec{r}_{\text{OH}_2}\left[\vec{F}_{\text{OH}_2}^{m(\text{cnstr.})}\cdot\left(\vec{v}_{\text{O}}, + \vec{v}_{\text{H}_2}\right)\right].\end{aligned} \tag{B5}$$

For TIP3P, an additional distance constraint is added between hydrogen atoms to maintain rigid body geometry, adding an additional term to Eq. (B5),

$$\begin{aligned}\vec{Q}^{\text{cnstr.(TIP3P)}} = &\frac{1}{2}\sum_{\substack{m=1 \\ \text{O},\text{H}_1,\text{H}_2\in m}}^{M}\vec{r}_{\text{OH}_1}\left[\vec{F}_{\text{OH}_1}^{m(\text{cnstr.})}\cdot\left(\vec{v}_{\text{O}} + \vec{v}_{\text{H}_1}\right)\right] \\ &+ \vec{r}_{\text{OH}_1}\left[\vec{F}_{\text{OH}_1}^{m(\text{cnstr.})}\cdot\left(\vec{v}_{\text{O}} + \vec{v}_{\text{H}_2}\right)\right] \\ &+ \vec{r}_{\text{H}_1\text{H}_2}\left[\vec{F}_{\text{H}_1\text{H}_2}^{m(\text{cnstr.})}\cdot\left(\vec{v}_{\text{H}_1} + \vec{v}_{\text{H}_2}\right)\right].\end{aligned} \tag{B6}$$

In case of TIP3P/rig, pairwise decomposition of apparent constraint forces is not readily available, therefore, we use the more general Eq. (A7) and substitute it to Eq. (A5),

$$\begin{aligned}\vec{Q}^{\text{cnstr.(TIP3P/rig)}} = &\sum_{\substack{m=1 \\ \text{O},\text{H}_1,\text{H}_2\in m}}^{M}\vec{r}_{\text{O}0}^{\,m}\otimes\vec{F}_{\text{O}}^{m(\text{cnstr.})}\cdot\vec{v}_{\text{O}} + \vec{r}_{\text{H}_1 0}^{\,m} \\ &\otimes\vec{F}_{\text{H}_1}^{m(\text{cnstr.})}\cdot\vec{v}_{\text{H}_1} + \vec{r}_{\text{H}_2 0}^{\,m}\otimes\vec{F}_{\text{H}_2}^{m(\text{cnstr.})}\cdot\vec{v}_{\text{H}_2}.\end{aligned} \tag{B7}$$

Note that while in Eqs. (B5) and (B6) notation $\vec{F}_{ij}^{m(\text{cnstr.})}$ indicates constrain force due to distance constraints between atoms i and j in molecule m, $\vec{F}_i^{m(\text{cnstr.})}$ in Eq. (B7) indicates total apparent constraint force on atom i in molecule m.

APPENDIX C: GROUP VIRIAL HEAT FLUX COMPONENT DEFINITIONS

In a similar manner to Appendix B, we will provide the definitions for the virial component of heat flux $\vec{Q}$ when using the group atomic virial stress form. The general expression of group form atomic stress is[4]

$$\boldsymbol{\sigma}_i^{\text{group}} = -\sum_{k=1}^{K_i}\frac{1}{N_k}\sum_{j\in k}\vec{r}_j\otimes\vec{F}_j^{k}, \tag{C1}$$

where the total virial for each many-body interaction k is first computed and then equally distributed to each participating atom. The pair and bond components $\vec{Q}^{\text{pair}}$ and $\vec{Q}^{\text{bond}}$ are identical to Eqs. (B2) and (B3) and will not be repeated. The angle component for TIP3P/Fs and TIP3P/Fs/cb can be obtained by substituting Eq. (C1) into Eq. (A5), which results in

$$\vec{Q}^{\text{angle}} = \sum_{\substack{k=1 \\ \text{O},\text{H}_1,\text{H}_2 \in k}}^{K(\text{angle})} \frac{1}{3}\left(\vec{r}_{\text{O}} \otimes \vec{F}_{\text{O}}^{k(\text{angle})} + \vec{r}_{\text{H}_1} \otimes \vec{F}_{\text{H}_1}^{k(\text{angle})} + \vec{r}_{\text{H}_2} \otimes \vec{F}_{\text{H}_2}^{k(\text{angle})}\right) \cdot (\vec{v}_{\text{O}} + \vec{v}_{\text{H}_1} + \vec{v}_{\text{H}_2}). \tag{C2}$$

In case of constraint force contribution in TIP3P/Fs/cb and TIP3P, as constraints are treated as many-body interactions in the original group formulation, the resulting definitions are different from centroid formulation where constraint forces could be treated as pairwise interactions. Specifically, the constraint force contributions for TIP3P/Fs/cb and TIP3P can be obtained by substituting Eq. (2) into Eq. (A5),

$$\vec{Q}^{\text{cnstr.(TIP3P/Fs/cb)}} = \frac{1}{3} \sum_{\substack{k=1 \\ \text{O},\text{H}_1,\text{H}_2 \in k}}^{M} \left(\vec{r}_{\text{OH}_1} \otimes \vec{F}_{\text{OH}_1}^{m(\text{cnstr.})} + \vec{r}_{\text{OH}_2} \otimes \vec{F}_{\text{OH}_2}^{m(\text{cnstr.})}\right) \cdot (\vec{v}_{\text{O}} + \vec{v}_{\text{H}_1} + \vec{v}_{\text{H}_2}), \tag{C3}$$

$$\vec{Q}^{\text{cnstr.(TIP3P)}} = \frac{1}{3} \sum_{\substack{m=1 \\ \text{O},\text{H}_1,\text{H}_2 \in m}}^{M} \left(\vec{r}_{\text{OH}_1} \otimes \vec{F}_{\text{OH}_1}^{m(\text{cnstr.})} + \vec{r}_{\text{OH}_2} \otimes \vec{F}_{\text{OH}_2}^{m(\text{cnstr.})} + \vec{r}_{\text{H}_1\text{H}_2} \otimes \vec{F}_{\text{H}_1\text{H}_2}^{m(\text{cnstr.})}\right) \cdot (\vec{v}_{\text{O}} + \vec{v}_{\text{H}_1} + \vec{v}_{\text{H}_2}). \tag{C4}$$

For constraint force component in rigid body dynamics, the constraint contribution is very similar to that of centroid definition in Eq. (B7), obtained by substituting Eq. (3) into Eq. (A5),

$$\vec{Q}^{\text{cnstr.(TIP3P/rig)}} = \sum_{\substack{m=1 \\ \text{O},\text{H}_1,\text{H}_2 \in m}}^{M} \vec{r}_{\text{O}} \otimes \vec{F}_{\text{O}}^{m(\text{cnstr.})} \cdot \vec{v}_{\text{O}} + \vec{r}_{\text{H}_1} \otimes \vec{F}_{\text{H}_1}^{m(\text{cnstr.})} \cdot \vec{v}_{\text{H}_1} + \vec{r}_{\text{H}_2} \otimes \vec{F}_{\text{H}_2}^{m(\text{cnstr.})} \cdot \vec{v}_{\text{H}_2}, \tag{C5}$$

where the only difference is that the absolute positional vectors are used. Note that due to an implementation detail in LAMMPS, Eq. (C5) is only strictly applied for the x component.

REFERENCES

[1]M. P. Allen and D. J. Tildesley, *Computer Simulation of Liquids* (Oxford University Press, 2009).
[2]D. Poulikakos and S. Maruyama, Microscale Thermophys. Eng. **7**, 181 (2003).
[3]S. Plimpton, J. Comput. Phys. **117**, 1 (1995).
[4]A. P. Thompson, S. J. Plimpton, and W. Mattson, J. Chem. Phys. **131**, 154107 (2009).
[5]Z. Fan, L. F. C. Pereira, H.-Q. Wang, J.-C. Zheng, D. Donadio, and A. Harju, Phys. Rev. B **92**, 094301 (2015).
[6]D. Surblys, H. Matsubara, G. Kikugawa, and T. Ohara, Phys. Rev. E **99**, 051301 (2019).
[7]P. Boone, H. Babaei, and C. E. Wilmer, J. Chem. Theory Comput. **15**, 5579 (2019).
[8]J.-P. Ryckaert, G. Ciccotti, and H. J. Berendsen, J. Comput. Phys. **23**, 327 (1977).
[9]H. C. Andersen, J. Comput. Phys. **52**, 24 (1983).
[10]A. V. Onufriev and S. Izadi, WIREs Comput. Mol. Sci. **8**, e1347 (2018).
[11]D. J. Evans and S. Murad, Mol. Phys. **68**, 1219 (1989).
[12]F. Müller-Plathe, J. Chem. Phys. **106**, 6082 (1997).
[13]P. Wirnsberger, D. Frenkel, and C. Dellago, J. Chem. Phys. **143**, 124104 (2015).
[14]W. L. Jorgensen, J. Chandrasekhar, J. D. Madura, R. W. Impey, and M. L. Klein, J. Chem. Phys. **79**, 926 (1983).
[15]U. W. Schmitt and G. A. Voth, J. Chem. Phys. **111**, 9361 (1999).
[16]Y. Wu, H. L. Tepper, and G. A. Voth, J. Chem. Phys. **124**, 024503 (2006).
[17]C. J. Fennell and J. D. Gezelter, J. Chem. Phys. **124**, 234104 (2006).
[18]P. H. Hünenberger, J. Chem. Phys. **116**, 6880 (2002).
[19]R. G. Winkler, J. Chem. Phys. **117**, 2449 (2002).
[20]T. Schneider and E. Stoll, Phys. Rev. B **17**, 1302 (1978).
[21]W. Shinoda, M. Shiga, and M. Mikami, Phys. Rev. B **69**, 134103 (2004).
[22]M. P. Allen and D. J. Tildesley, *Computer Simulation of Liquids* (Oxford University Press, 2009), pp. 192–195.
[23]M. P. Allen and D. J. Tildesley, *Computer Simulation of Liquids* (Oxford University Press, 2009), pp. 46–50.
[24]B. Hess, H. Bekker, H. J. C. Berendsen, and J. G. E. M. Fraaije, J. Comput. Chem. **18**, 1463 (1997).
[25]H. Matsubara, G. Kikugawa, M. Ishikiriyama, S. Yamashita, and T. Ohara, J. Chem. Phys. **147**, 114104 (2017).
[26]E. A. Algaer and F. Müller-Plathe, Soft Mater. **10**, 42 (2012).
[27]M. L. V. Ramires, C. A. Nieto de Castro, Y. Nagasaka, A. Nagashima, M. J. Assael, and W. A. Wakeham, J. Phys. Chem. Ref. Data **24**, 1377 (1995).
[28]Y. Mao and Y. Zhang, Chem. Phys. Lett. **542**, 37 (2012).
[29]T. W. Sirk, S. Moore, and E. F. Brown, J. Chem. Phys. **138**, 064505 (2013).
[30]N. J. English, Mol. Phys. **106**, 1887 (2008).
[31]J. Muscatello and F. Bresme, J. Chem. Phys. **135**, 234111 (2011).
[32]H. J. C. Berendsen, J. R. Grigera, and T. P. Straatsma, J. Phys. Chem. **91**, 6269 (1987).
[33]T. Ohara, J. Chem. Phys. **111**, 6492 (1999).
[34]H. Matsubara, G. Kikugawa, and T. Ohara, Int. J. Therm. Sci. **161**, 106762 (2021).
[35]E. Krieger and G. Vriend, J. Comput. Chem. **36**, 996 (2015).
[36]D. Torii, T. Nakano, and T. Ohara, J. Chem. Phys. **128**, 044504 (2008).